Unmasking Bulk Exciton Traps and Interchain Electronic Interactions with Single Conjugated Polymer Aggregates

Matthew C. Traub,[†] Jan Vogelsang,[†,⊥] Kyle N. Plunkett,[‡,¶] Colin Nuckolls,[‡] Paul F. Barbara,[†,§] and David A. Vanden Bout*[,†]

[†]Department of Chemistry and Biochemistry and the Center for Nano and Molecular Science and Technology, The University of Texas at Austin, Austin, Texas 78712, United States, and [‡]Department of Chemistry, Columbia University, New York, New York 10027, United States. [§]Paul Barbara passed away on October 31, 2010. [⊥]Present address: Institut für Experimentelle und Angewandte Physik, Universität Regensburg, D-93053 Regensburg. [¶]Present address: Department of Chemistry and Biochemistry, Southern Illinois University, Carbondale, Illinois, 62901.

ABSTRACT For conjugated polymer materials, there is currently a major gap in understanding between the fundamental properties observed in single molecule measurements and the bulk electronic properties extracted from measurements of highly heterogeneous thin films. New materials and methodologies are needed to follow the evolution from single chain to bulk film properties as multiple chains begin to interact. In this work, we used a controlled solvent vapor annealing process to assemble single chains of phenylene–vinylene conjugated polymers into aggregates that can be individually spectroscopically interrogated. This approach allowed us to probe the effects of interchain coupling in isolated conjugated polymer nanodomains of controlled size. By assembling these aggregates from building blocks of both pristine MEH–PPV and MEH–PPV derivatives containing structure-directing *ortho*- or *para*-terphenyl inclusions, we were able to control the ordering of these nanodomains as measured by single aggregate polarization anisotropy measurments. Depending on the individual chain constituents, these aggregates varied from highly anisotropic to nearly isotropic, respectively facilitating or inhibiting interchain coupling. From the single chain fluorescence lifetimes, we demonstrated that these structure directing inclusions effectively break the phenylene–vinylene conjugation, allowing us to differentiate interchain electronic effects from those due to hyper-extended conjugation. We observed well-defined bathochromic shifts in the fluorescence spectra of the aggregates containing extensive interchain interactions, indicating that low-energy exciton traps in MEH–PPV are the result of coupling interactions between neighboring chain segments. These results demonstrate the power of the synthetic inclusion approach to control properties at not just the single chain level, but as a comprehensive approach toward ground-up design of bulk electronic properties.

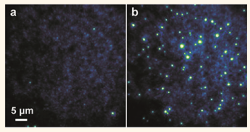

KEYWORDS: conjugated polymers · organic electronics · photoluminescence · self-assembly · structure–property relationships

A major obstacle to the rational design of conjugated polymer (CP) films for use in photovoltaic and light-emitting diode devices is the difficulty of understanding the relationship between morphology and energy trapping in these materials.[1,2] Disorder and formation of exciton or polaron trap sites can inhibit the flow of energy through CP films, drastically altering their performance.[3−5] Because these films are heterogeneous and the morphological features that lead to these defects are smaller than the diffraction limit of light ($\sim\lambda/2$), single molecule spectroscopy (SMS) has been extensively employed for the study of CP morphology.[6,7] While charge trapping[8,9] and energy trapping sites[10] can form even at the level of single CP chains, interchain interactions are likely to introduce new states in these materials and potentially dominate their bulk behavior.[11] The underlying physical structure of these interactions and their relationship to trapping in bulk films is still the subject of much debate, and new approaches are necessary to bridge the gap between single molecule and bulk studies.

Previous attempts to understand CP morphology at the single chain level have largely relied on excitation polarization anisotropy.[12−15] As linearly polarized excitation is rotated 180° in the sample plane, the fluorescence intensity is recorded and the resulting data is fit to

$$I(\theta) \propto 1 + M \cos 2(\theta - \varphi) \qquad (1)$$

where θ is the phase of the incident light, ϕ is the angle where emission intensity is maximized, and M is the modulation depth. The parameter M, the in-plane projection of the anisotropy, corresponds to the overall alignment of each chain. For high-quality samples of the prototypical fluorescent conjugated polymer poly[2-methoxy-5-(2′-ethyhexyloxy)]−1,4-phenylenevinylene (MEH–PPV), high values of M (>0.6) reveal that the majority of MEH–PPV single chains spun-cast from toluene solution in an inert poly(methyl methacrylate) (PMMA) matrix spontaneously organize into highly ordered,

* Address correspondence to davandenbout@mail.utexas.edu.

Received for review October 6, 2011 and accepted December 19, 2011.

Published online December 30, 2011
10.1021/nn203860u

rodlike structures during the spin-coating process.[13,16,17] Recent work has demonstrated that solvent vapor annealing (SVA) of PMMA films containing single MEH–PPV chains in a N_2 atmosphere saturated with a solvent mixture of acetone (in which the PMMA host is highly soluble and the MEH–PPV sparingly soluble) and chloroform (in which are both highly soluble), leads to the formation of organized CP aggregates.[18] Because the average separation between the aggregates is greater than the optical diffraction limit, each one can be individually spectroscopically interrogated. Despite containing 20–25 MEH–PPV chains, depending on the ratio of acetone to chloroform and the starting MEH–PPV concentration, these aggregates have an average excitation polarization anisotropy of ~0.6. The organization of these SVA formed aggregates suggests that there is a strong driving force for alignment along the backbones of the individual rodlike chains, providing an ideal environment to probe the formation of bulk electronic properties.

In this work, we use the SVA process to assemble aggregates of pristine MEH–PPV and two MEH–PPV derivatives that synthetically incorporate structure-directing units. By replacing 30% of the MEH–PPV monomers with *ortho*- or *para*-terphenyl inclusions, rigid groups that kink the chain or force it to be linear,[19] we disrupt the backbone conjugation and provide for rational control of interchain interactions. The rigid terphenyl groups, randomly incorporated as 30% of the overall monomers, either hold the individual chains linear and prevent bends (*para*-terphenyl) or force the chain backbone to fold back and prevent highly extended linear phenylene–vinylene segments from forming (*ortho*-terphenyl). Thus, during aggregate formation, stacking interactions between neighboring chains in the para-inclusion CPs will be more sterically favorable than in pristine MEH–PPV. This is in contrast to the ortho-inclusion CPs, where these interactions will be more unfavorable compared to pristine MEH–PPV. Single molecule and single aggregate spectroscopic measurements of these materials allow us to draw direct correlations between structure and the formation of low-energy traps and demonstrate the potential for engineering bulk film properties by systematic inclusion of structure directing monomers.

RESULTS AND DISCUSSION

Spin-cast films of PMMA containing isolated single chains of CPs were annealed in an N_2 atomosphere saturated with acetone/chloroform in an 80:20 ratio. For both pristine MEH–PPV and the inclusion polymers, wide field fluorescence images contained fewer spots after the SVA process with substantially greater average brightness for each spot (Figure 1). Previous observations of pristine MEH–PPV at a constant excitation rate estimated 20–25 chains per aggregate based on mean intensity increase for the excitation conditions

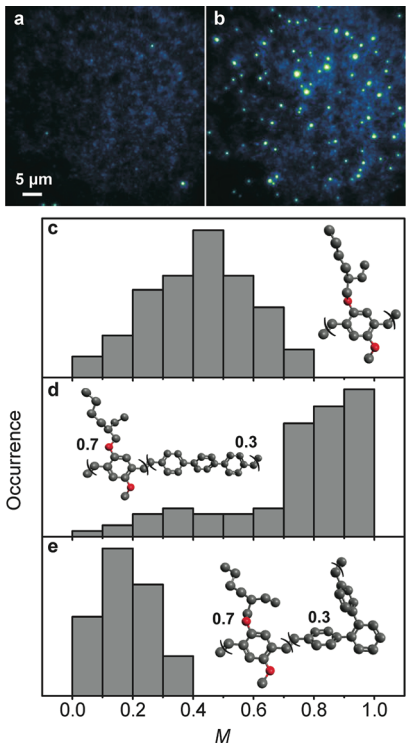

Figure 1. Wide-field fluorescence images of MEH–PPV (a) before and (b) after solvent vapor annealing in 80:20 acetone/chloroform. Polarization anisotropy probability histograms for (a) pristine, (b) 30% *para*-terphenyl, and (c) 30% *ortho*-terphenyl MEH–PPV were measured for 150–300 aggregates. The mean modulation depths were 0.42, 0.76, and 0.18, respectively. Histogram insets show the structure of each polymer.

and molecular weight described in reference 18. We found that aggregates of both terphenyl containing CPs were more susceptible to photo-oxidation and blinking/bleaching than MEH–PPV. To avoid these complications, we performed the polarization anisotropy measurements at a lower excitation intensity (~10 W cm^{-2} for aggregates *vs* ~50 W cm^{-2} for single molecules), and we have not attempted to make a direct comparison between the number and intensity of spots in single molecule images in the current work. All comparisons between aggregates were made using brightness thresholds set to give I_{mean} = 10000 counts, ensuring that observed anisotropy differences are primarily due to the actual alignment of the polymer chains within single domains and are not distorted by the possibility that one sample contains larger aggregates with multiple internally aligned domains.[18]

Polarization anisotropy measurements of the aggregates show that the rigid para-inclusion polymers are even more highly ordered than the pristine polymer, with a mean *M* of 0.76 indicating nearly perfect alignment of the individual chain backbones along the major axis of the aggregate. In contrast, the ortho-inclusion aggregates are nearly completely isotropic, with a mean *M* of 0.18. These results confirm a picture of MEH–PPV aggregation in which the organization is driven by favorable interaction between linear

chromophore units on neighboring chains. In the para-inclusion CP, the *para*-terphenyl groups hold each individual chain in an extended linear conformation,[19] and allow multiple contacts per chain. The electronic or steric effects of these chains force nearby chains to become more linear to facilitate packing, eliminating many of the lower *M* values observed in the single molecule histogram[19] and yielding a narrower distribution. The *ortho*-terphenyl groups, chosen to simulate the effects of cis-defects in the backbone, randomly bend the chain and were observed to result in more disordered single chain nanostructures.[19] Because of the dispersion in both chain lengths and number of defects per chain (30% is the average number of inclusions per chain), the overall distribution *M* values were quite broad for the single chains with ortho inclusions. These inclusions make the interchain packing interactions sterically inaccessible, and the aggregates are composed of multiple, randomly aligned nanodomains narrowly clustered around small *M* values. The lower mean (M = 0.42, compared to M = 0.74 in ref 18) and broader distribution observed for pristine MEH–PPV in this work is likely caused by selection against the smallest, most-aligned aggregates at the lower excitation power used in these experiments and the lower molecular weight (16 kDa, compared to 830 kDa in ref 18), which potentially leads to more chains per aggregate and formation of multiple, randomly oriented domains.

The structural diversity of these aggregates provides a unique opportunity to probe the effects of morphology and interchain interactions on the electronic structure and spectroscopic properties of MEH–PPV with single molecule spectroscopy at the mesoscopic length scale. The room temperature solution emission spectrum of pristine MEH–PPV is peaked at 550–560 nm,[20] while the thin film spectrum is peaked at ~585 nm.[21,22] The single molecule emission peaks are known to be bimodally distributed between these two "blue" and "red" values.[23–26] Efficient energy transfer between chromophore segments in the chain results in exciton funneling to red sites in single chains,[27] implicating them as a major source of energy trapping in films. Recent work by Feist and Basché showed that low molecular weight (M_n = 50k) chains are exclusively blue,[28] an observation that held for the lower molecular weight MEH–PPV used in this work (M_n = 16k) (Figure 2). However, the emission spectra of the MEH–PPV aggregates are uniformly shifted to red values. The narrower distribution observed in the probability histogram of peak energies for the aggregates relative to the single molecules was primarily due to their greater brightness and improved signal-to-noise ratio.

The ensemble single molecule emission spectra of the para-inclusion polymer is peaked at 536 nm (Figure 2), which is 10 nm blue-shifted of the pristine ensemble peak at 546 nm. This shift is consistent with the 10-nm hypsochromic shift of the solution emission

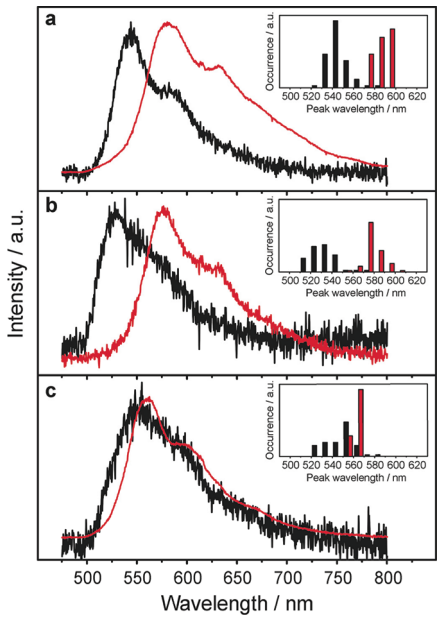

Figure 2. Photoluminescence spectra for (a) pristine, (b) 30% *para*-terphenyl, and (c) 30% *ortho*-terphenyl MEH–PPV excited at 488 nm. Ensemble single molecule spectra are in black and ensemble single aggregate spectra are in red. Insets show histograms of single molecule/aggregate peak wavelengths for the 50–70 single spectra collected for each sample.

spectra for the 30% terphenyl polymers relative to pure MEH–PPV due to their shorter effective conjugation length.[19] The random incorporation of the terphenyl units leads to a much broader distribution of chromophore lengths than in pristine MEH–PPV, and a correspondingly broader distribution of single molecule peak energies. The ~40 nm bathochromic shift of the para-aggregates (ensemble λ_{max} = 578 nm) is nearly identical to that observed for pristine MEH–PPV, indicating that it is caused by the same underlying interchain interactions. The narrowing of the peak energies suggests a high degree of uniformity in the nature of the low-energy sites formed during aggregation.

In contrast, the peak energies for the ortho-inclusion single molecules are more dispersed, leading to a broadened ensemble spectrum. Individual spectra have the same broadening and vibronic structure observed in single molecules of the para-inclusion and pristine polymers (Figure 3). Despite having a solution emission spectrum similar to the para-inclusion polymer, their single molecule emission spectrum is peaked at ~20 and ~10 nm red-shifted of the para-inclusions and pristine single molecules, respectively. The corresponding ortho-inclusion aggregates are bathochromically shifted <10 nm, with a peak histogram clustered around the lowest energy single molecule peaks. These results strongly suggest that the bends imposed by the *ortho*-terphenyl groups force limited interchain interactions to form during the spin-coating process, but prevent extended interchain interactions. The morphology of the ortho-inclusion

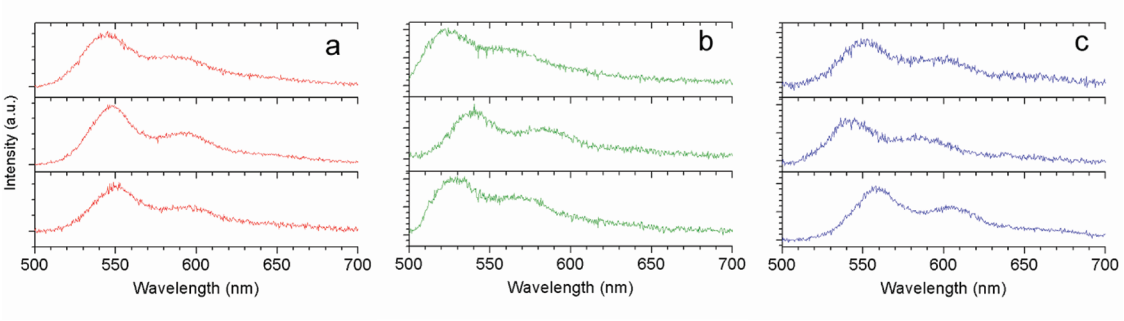

Figure 3. Representative single molecule fluorescence spectra for (a) pristine MEH−PPV, (b) 30% *para*-terphenyl and (c) 30% *ortho*-terphenyl. Similar vibronic progressions are observed for all three species despite the greater variation in peak energy for the 30% *ortho*-terphenyl relative to the 30% *para*-terphenyl or pristine MEH−PPV chains.

polymers is formed at the single chain level, with each single chain comprising a nanodomain within an aggregate and having limited interaction with its neighbors.

We analyzed the spectral line shapes of individual single molecules and aggregates to avoid broadening due to the distribution of 0−0 energy gaps in the ensemble spectrum. Individual spectra could all be represented by a Franck−Condon progression of vibronic peaks,[23,29] and the fits showed only minor differences in vibronic spacing and Huang−Rhys factors. While the longer effective conjugation length in the pristine aggregates may lead to subtle changes in spectral shape, such changes in peak shape are difficult to discern from measurements on conjugated polymers collected at room temperature.[30]

The correlation between spectra and morphology of these polymer aggregates allows new insight into the formation of low energy traps in polymer films. Potential mechanisms for the formation of low energy sites include excimer formation, interchain dipole−dipole or electronic coupling, and a conformational change in the geometry of chain chromophore segments caused by interchain steric interactions. Interchain excimer emission is characterized by broad, featureless emission,[31] in contrast to the well-resolved vibronic features observed for these aggregates, and the magnitude of the bathochromic shift (~1300 cm^{-1}) is too small for strong electronic coupling.[32] For phenylene−vinylenes, interchain dipole coupling of cofacial chains reduces the intensity of the S_0−S_1 transition,[32] but puts significant strength into the S_0−S_2 transition.[33] These effects lead to a significantly reduced quantum yield, and would seem inconsistent with the para-inclusion aggregates, which are both highly aligned and of comparable brightness to the other samples. However, the alkoxy side chains of the polymers are regiorandom, and may break the symmetry enough to maintain significant oscillator strength in the S_0−S_1 transition.

Planarization of chromophores to extend the effective conjugation length is well-established in the formation of β phase poly(9,9-dioctyl)fluorene (PFO),[34,35] and hyper-extended exciton delocalization in PFO has been reported at the single chain level.[36] While hyper-extended conjugation is possible in the pristine

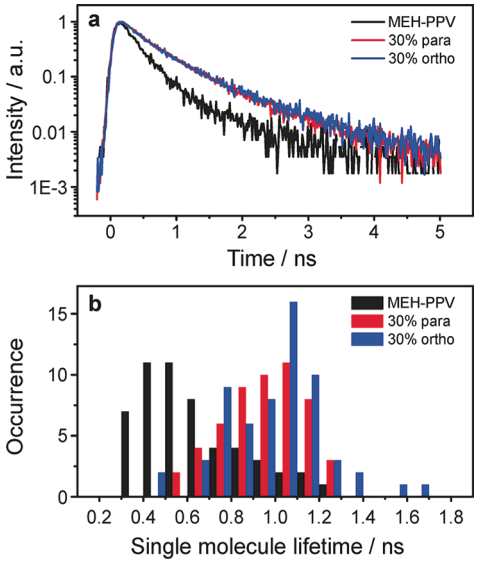

Figure 4. (Top) Solution lifetimes of the CPs measured in toluene were were 350, 570, and 580 ps for the pristine, *para*-terphenyl and *ortho*-terphenyl MEH−PPV, respectively. (Bottom) Histogram of single molecule lifetimes. The mean single molecule lifetimes were 620 ps (pristine), 940 ps (para), and 990 ps (ortho).

MEH−PPV, exciton delocalization should be limited by the terphenyl groups in the para-inclusion polymer, as suggested by its hypsochromically shifted solution fluorescence.[19] To further verify that the terphenyl groups effectively break the phenylene−vinylene conjugation, we measured the ensemble solution and single molecule lifetimes of all three compounds (Figure 4). The fluorescence lifetimes were fit to single exponentials. Biexponential fits of the solution decays showed long-lived components contributing less than 1% of the observed intensity. While the mean lifetimes for all of the polymers increase from solution to single molecules in the solid state, the solution and mean single molecule lifetimes of the inclusion polymers are consistently ~300 ps longer than those of pristine MEH−PPV. Oscillator strength in oligophenylene−vinylenes and PPVs is well-known to increase linearly with conjugation length, leading to longer lifetimes for shorter chromophores.[37,38] These data further suggest

that conjugation is effectively broken by the synthetic inclusions. The distribution of single molecule lifetimes was broader for both of the inclusion polymers due to variations in the position and total number of terphenyl inclusions per chain, which results in substantial chain-to-chain variance in the length of the lowest energy chromophores. Highly extended conjugation may be present in the pristine MEH–PPV aggregates, leading to a slightly lower-energy ensemble emission peak than for the para-inclusion aggregates, but it does not appear to be necessary to generate similar bathochromic shifts.

The lifetimes of the terphenyl-inclusion aggregates could not be fit by simple first order kinetics. The susceptibility of the aggregates to photoxidation led to blinking or photobleaching within 2–3 s, and the corresponding appearance of short-lived components (τ < 250 ps) in the decay curves. These fast-decay components are consistent with previous observations of drastically shortened lifetimes during blinking events in MEH–PPV single molecules.[14,27] In contrast, blinking or bleaching during the collection of single aggregate spectra led to a loss of intensity but not a change in spectral features, allowing us to collect spectral data with good signal-to-noise. We hypothesize that trapped polarons formed during blinking or bleaching introduce a rapid nonradiative decay pathway for the fraction of the aggregate that is able to efficiently transfer energy to the quencher. The convolution of photochemistry and intrinsic photophysics in the aggregates inhibited the direct comparison of fluorescence lifetimes in aggregates to those in single molecules or solution. Developing a more detailed understanding of the nonradiative decay kinetics in these aggregates represents ongoing research in our group.

These results are consistent with previous studies with oligomer models for MEH–PPV[39] and strongly suggest that red sites in single molecules of MEH–PPV originate in intrachain interactions between segments of single polymer chains. For low molecular weight samples, the chain adopts an extended conformation and shows only blue emission. At some molecular weight above 50 kDa,[28] it is able to fold back on itself and form hairpin structures, allowing interactions to occur between segments. This hairpin model is consistent with both reported spectral data and the extended, needle-like structures observed for high molecular weight (M_n > 800 kDa) MEH–PPV single molecules.[16]

CONCLUSIONS

This work describes the self-assembly of aggregates of MEH–PPV and MEH–PPV derivatives containing structure directing inclusions by a solvent vapor annealing process. By synthetically defining the polymer backbone rigidity and linearity, we were able to rationally control the extent of interchain interactions and the corresponding ordering of individual polymer nanodomains. This ordering varied from nearly completely aligned for *para*-terphenyl containing MEH–PPV to nearly completely isotropic for *ortho*-terphenyl containing MEH–PPV. Measurement of the fluorescence spectra showed well-defined bathochromic shifts between single molecules and single aggregates for the *para*-terphenyl and pristine MEH–PPV, which contained extensive interchain interactions. In contrast, for the *ortho*-terphenyl MEH–PPV, no such interactions could be formed and no corresponding shift was observed. Single molecule fluorescence lifetime measurements confirmed that the terphenyl groups effectively broke the backbone phenylene–vinylene conjugation. These results strongly imply that interchromophore dipole or electronic coupling, not hyperextended conjugation, is primarily responsible for the formation of energy trapping red sites in both single molecules and bulk films.

The simultaneous control of conjugated polymer self-assembly process and backbone inclusions presented in this work holds significant promise for improved CP film properties. Highly aligned single polymer nanodomains facilitate ultralong range energy transfer,[9] and rigid synthetic inclusions like *para*-terphenyl could be used to increase exciton diffusion lengths in organic photovoltaics. For organic light-emitting diodes, increased film disorder and fewer interchain interactions lead to a reduction in exciton quenching, and *ortho*-terphenyl-type inclusions are candidates for increasing their electroluminescence efficiency. Finally, the hopping transport of charges in CP thin films is enhanced by a narrow, uniform density of states,[40] and ground up control of chromophore length and morphology is a critical step toward optimizing films with improved electrical transport. Given that different applications can require distinct physical, optical, and electronic properties, the ability to rationally design conjugated polymers with controlled morphology and assemble these polymers into well-defined domains with predictable electronic properties is a critical step in the development of the next generation of organic electronic devices.

MATERIALS AND METHODS

Sample Preparation. To prevent oxidation, all single molecule samples were prepared in an inert atmosphere glovebox. Poly[2-methoxy-5-(2′-ethylhexyloxy)1,4-phenylenevinylene] (MEH–PPV) (M_n = 16900, PDI = 2.1) and 30% *ortho*-terphenyl (M_n = 11700, PDI = 1.5) and 30% *para*-terphenyl (M_n = 25300, PDI = 2.0) substituted derivatives were synthesized as described previously.[19] Poly(methyl methacrylate) (PMMA) (Sigma Aldrich, M_n = 45 kDa, PDI = 2.2) was used as received. Glass coverslips were cleaned with piranha solution (sulfuric acid/hydrogen peroxide in 3:1 v/v ratio) for a minimum of 1 h before use. Solutions of conjugated polymer and 6% wt. PMMA in anhydrous toluene (99.8%, Acros) were dynamically spin-cast on

glass coverslips at 2000 rpm, yielding 200 nm PMMA films containing isolated polymer chains. For single molecule experiments, the concentration of conjugated polymer in solution was $\sim 10^{-14}$ M, leading to a final film density of *ca.* 0.01−0.02 spots um^{-2}. Before measurement, all samples were sealed from ambient atmosphere using epoxy and a glass coverslip or a home-built gas flow cell that was continuously purged with N_2-gas. To prepare solvent vapor annealed aggregates, films were cast from ~500× more concentrated solution ($\sim 5 \times 10^{-11}$ M), and the N_2 gas was saturated with anhydrous chloroform−acetone (Acros) by slowly purging it through a solvent reservoir. The solvent ratio in the reservoir was calculated to yield a vapor phase ratio of 20:80 (chloroform/acetone) from the vapor phase diagram at 22 °C.

Polarization Anisotropy and Emission Spectra. The microscope apparatus for polarization modulation and apparatus for single molecule spectra have been described in detail previously.[13] For polarization anisotropy measurements, linearly polarized light from the 488 nm line of an Ar ion laser (Melles-Griot, 35 LAL-030-208) was focused into the back of the microscope objective (Zeiss, 100×, NA 1.25), filtered, and focused onto an EM-CCD camera (Andor, iXon$^+$ DU-897E). The polarization of the light was modulated with an electro-optic modulator (Fastpulse 3079) driven by high-voltage power supply and function generator. For spectra, circularly polarized light from the 488-nm line of laser was focused onto the sample, which was scanned with a piezoelectric stage (Queensgate). Collected light was filtered through a notch and passed through a monochromator (Acton, SP-150) onto a CCD spectrometer (Princeton Instruments, LN/CCD-1340). For each sample, 50−70 single molecule or aggregate spectra were collected.

Fluorescence Lifetimes. Laser light ($\lambda_{ex} = 473$ nm) from a pulsed diode laser (Becker & Hickl GmbH, BDL-473-SMC) operating at 50 MHz, was passed through a $\lambda/4$ wave plate, reflected off a dichroic mirror, and focused through the objective (Zeiss, 100× ApoPlano 1.4 NA) of an inverted fluorescence microscope (Zeiss, Axiovert 100) on to the samples, which were scanned with a piezoelectric stage. Emitted light was passed through a 514 nm Raman edge filter and focused on to an avalanche photodiode (APD) (ID Quantique, id100-50). The signal from the APD was simultaneously sent to a time correlated single photon counting (TCSPC) board (Becker & Hickl GmbH, SPC-830) and a multichannel scanner (MCS) board (Becker & Hickl GmbH, PMS-400A). The transient from the MCS was monitored for photochemical events, and molecules that showed blinking or photobleaching during TCSPC collection were not included in the analysis. The instrument response function (IRF) of the system, measured from reflected laser light by removing the Raman edge filter, was found to be 52 ps. The IRF was deconvoluted from the measured decay curves during fitting in Origin 7.0.

Acknowledgment. This work was supported as part of the program "Molecular Tools for Conjugated Polymer Analysis and Optimization", a Center for Chemical Innovation (CCI, phase 1) under NSF Award No. CHE-0943957. J. Vogelsang thanks the German Research Foundation (DFG) for a fellowship. We thank Takuji Adachi for help with the initial aggregate experiments and Johanna Brazard for her help with deconvolution of the lifetime decays and with the spectrometer.

REFERENCES AND NOTES

1. Westenhoff, S.; Howard, I. A.; Friend, R. H. Probing the Morphology and Energy Landscape of Blends of Conjugated Polymers with Sub-10 nm Resolution. *Phys. Rev. Lett.* **2008**, *101*, 016102.
2. McNeill, C. R.; Watts, B.; Thomsen, L.; Ade, H.; Greenham, N. C.; Dastoor, P. C. X-ray Microscopy of Photovoltaic Polyfluorene Blends: Relating Nanomorphology to Device Performance. *Macromolecules* **2007**, *40*, 3263–3270.
3. Ma, W. L.; Yang, C. Y.; Gong, X.; Lee, K.; Heeger, A. J. Thermally Stable, Efficient Polymer Solar Cells with Nanoscale Control of the Interpenetrating Network Morphology. *Adv. Funct. Mater.* **2005**, *15*, 1617–1622.
4. Hoffmann, S. T.; Scheler, E.; Koenen, J. M.; Forster, M.; Scherf, U.; Strohriegl, P.; Bassler, H.; Kohler, A. Triplet Energy Transfer in Conjugated Polymers. III. An Experimental Assessment Regarding the Influence of Disorder on Polaronic Transport. *Phys. Rev. B* **2010**, *81*, 165208.
5. Feast, W. J.; Cacialli, F.; Koch, A. T. H.; Daik, R.; Lartigau, C.; Friend, R. H.; Beljonne, D.; Bredas, J.-L. Control of Luminescence in Conjugated Polymers Through Control of Chain Microstructure. *J. Mater. Chem.* **2007**, *17*, 907–912.
6. Barbara, P. F.; Gesquiere, A. J.; Park, S.-J.; Lee, Y. J. Single-Molecule Spectroscopy of Conjugated Polymers. *Acc. Chem. Res.* **2005**, *38*, 602–610.
7. Lupton, J. M. Single-Molecule Spectroscopy for Plastic Electronics: Materials Analysis from the Bottom-up. *Adv. Mater.* **2010**, *22*, 1689–1721.
8. Bolinger, J. C.; Fradkin, L.; Lee, K. J.; Palacios, R. E.; Barbara, P. F. Light-Assisted Deep-Trapping of Holes in Conjugated Polymers. *Proc. Natl. Acad. Sci. U.S.A.* **2009**, *106*, 1342–1346.
9. Bolinger, J. C.; Traub, M. C.; Adachi, T.; Barbara, P. F. Ultra-long-Range Polaron-Induced Quenching of Excitons in Isolated Conjugated Polymers. *Science* **2011**, *331*, 565–567.
10. Feist, F. A.; Zickler, M. F.; Basché, T. Origin of the Red Sites and Energy Transfer Rates in Single MEH−PPV Chains at Low Temperature. *ChemPhysChem* **2011**, 1499–1508.
11. Blatchford, J. W.; Jessen, S. W.; Lin, L. B.; Gustafson, T. L.; Fu, D. K.; Wang, H. L.; Swager, T. M.; MacDiarmid, A. G.; Epstein, A. J. Photoluminescence in Pyridine-Based Polymers: Role of Aggregates. *Phys. Rev. B* **1996**, *54*, 9180–9189.
12. Hu, D. H.; Yu, J.; Wong, K.; Bagchi, B.; Rossky, P. J.; Barbara, P. F. Collapse of Stiff Conjugated Polymers with Chemical Defects into Ordered, Cylindrical Conformations. *Nature* **2000**, *405*, 1030–1033.
13. Adachi, T.; Brazard, J.; Chokshi, P.; Bolinger, J. C.; Ganesan, V.; Barbara, P. F. Highly Ordered Single Conjugated Polymer Chain Rod Morphologies. *J. Phys. Chem. C* **2010**, *114*, 20896–20902.
14. Lin, H.; Tabaei, S. R.; Thomsson, D.; Mirzov, O.; Larsson, P.-O.; Scheblykin, I. G. Fluorescence Blinking, Exciton Dynamics, and Energy Transfer Domains in Single Conjugated Polymer Chains. *J. Am. Chem. Soc.* **2008**, *130*, 7042–7051.
15. Ebihara, Y.; Vacha, M. Relating Conformation and Photophysics in Single MEH−PPV Chains. *J. Phys. Chem. B* **2008**, *112*, 12575–12578.
16. Traub, M. C.; Lakhwani, G.; Bolinger, J. C.; Bout, D. V.; Barbara, P. F. Electronic Energy Transfer in Highly Aligned MEH−PPV Single Chains. *J. Phys. Chem. B* **2011**, *115*, 9941–9947.
17. Habuchi, S.; Onda, S.; Vacha, M. Molecular Weight Dependence of Emission Intensity and Emitting Sites Distribution within Single Conjugated Polymer Molecules. *Phys. Chem. Chem. Phys.* **2011**, *13*, 1743–1753.
18. Vogelsang, J.; Adachi, T.; Brazard, J.; Bout, D. V.; Barbara, P. F. Self-Assembly of Highly Ordered Conjugated Polymer Aggregates with Long-Range Energy Transfer. *Nat. Mater.* **2011**, *10*, 942–946.
19. Bounos, G.; Ghosh, S.; Lee, A. K.; Plunkett, K. N.; DuBay, K. H.; Bolinger, J. C.; Zhang, R.; Friesner, R. A.; Nuckolls, C.; Reichman, D. R.; *et al.* Controlling Chain Conformation in Conjugated Polymers Using Defect Inclusion Strategies. *J. Am. Chem. Soc.* **2011**, *133*, 10155–10160.
20. Padmanaban, G.; Ramakrishnan, S. Conjugation Length Control in Soluble Poly[2-methoxy-5-((2′-ethylhexyl)oxy)-1,4-phenylenevinylene] (MEHPPV): Synthesis, Optical Properties, and Energy Transfer. *J. Am. Chem. Soc.* **2000**, *122*, 2244–2251.
21. Gaab, K. M.; Bardeen, C. J. Wavelength and Temperature Dependence of the Femtosecond Pump-Probe Anisotropies in the Conjugated Polymer MEH−PPV: Implications for Energy-Transfer Dynamics. *J. Phys. Chem. B* **2004**, *108*, 4619–4626.
22. Nguyen, T.-Q.; Martini, I. B.; Liu, J.; Schwartz, B. J. Controlling Interchain Interactions in Conjugated Polymers: The Effects of Chain Morphology on Exciton−Exciton Annihilation and Aggregation in MEH−PPV Films. *J. Phys. Chem. B* **2000**, *104*, 237–255.

23. Kim, D. Y.; Grey, J. K.; Barbara, P. F. A Detailed Single Molecule Spectroscopy Study of the Vibronic States and Energy Transfer Pathways of the Conjugated Polymer MEH−PPV. *Synth. Met.* **2006**, *156*, 336–345.
24. Lee, Y. J.; Kim, D. Y.; Barbara, P. F. Effect of Sample Preparation and Excitation Conditions on the Single Molecule Spectroscopy of Conjugated Polymers. *J. Phys. Chem. B* **2006**, *110*, 9739–9742.
25. Grey, J. K.; Kim, D. Y.; Donley, C. L.; Miller, W. L.; Kim, J. S.; Silva, C.; Friend, R. H.; Barbara, P. F. Effect of Temperature and Chain Length on the Bimodal Emission Properties of Single Polyfluorene Copolymer Molecules. *J. Phys. Chem. B* **2006**, *110*, 18898–18903.
26. Ebihara, Y.; Habuchi, S.; Vacha, M. Conformation-Dependent Room-Temperature Emission Spectra of Single MEH−PPV Chains in Different Polymer Matrices. *Chem. Lett.* **2009**, *38*, 1094–1095.
27. Yu, J.; Hu, D.; Barbara, P. F. Unmasking Electronic Energy Transfer of Conjugated Polymers by Suppression of O_2 Quenching. *Science* **2000**, *289*, 1327–1330.
28. Feist, F. A.; Basche, T. Fluorescence Excitation and Emission Spectroscopy on Single MEH−PPV Chains at Low Temperature. *J. Phys. Chem. B* **2008**, *112*, 9700–9708.
29. Hagler, T. W.; Pakbaz, K.; Voss, K. F.; Heeger, A. J. Enhanced Order and Electronic Delocalization in Conjugated Polymers Oriented by Gel Processing in Polyethylene. *Phys. Rev. B* **1991**, *44*, 8652–8666.
30. Clark, J.; Silva, C.; Friend, R. H.; Spano, F. C. Role of Intermolecular Coupling in the Photophysics of Disordered Organic Semiconductors: Aggregate Emission in Regioregular Polythiophene. *Phys. Rev. Lett.* **2007**, *98*, 206406.
31. Lemmer, U.; Heun, S.; Mahrt, R. F.; Scherf, U.; Hopmeier, M.; Siegner, U.; Gobel, E. O.; Mullen, K.; Bassler, H. Aggregate Fluorescence in Conjugated Polymers. *Chem. Phys. Lett.* **1995**, *240*, 373–378.
32. Cornil, J.; Heeger, A. J.; Bredas, J. L. Effects of Intermolecular Interactions on the Lowest Excited State in Luminescent Conjugated Polymers and Oligomers. *Chem. Phys. Lett.* **1997**, *272*, 463–470.
33. Sterpone, F.; Bedard-Hearn, M. J.; Rossky, P. J. Nonadiabatic Mixed Quantum-Classical Dynamic Simulation of π-Stacked Oligophenylenevinylenes. *J. Phys. Chem. A* **2009**, *113*, 3427–3430.
34. Grell, M.; Bradley, D. D. C.; Ungar, G.; Hill, J.; Whitehead, K. S. Interplay of Physical Structure and Photophysics for a Liquid Crystalline Polyfluorene. *Macromolecules* **1999**, *32*, 5810–5817.
35. Chunwaschirasiri, W.; Tanto, B.; Huber, D. L.; Winokur, M. J. Chain Conformations and Photoluminescence of Poly(di-*n*-octylfluorene). *Phys. Rev. Lett.* **2005**, *94*, 107402.
36. Da Como, E.; Borys, N. J.; Strohriegl, P.; Walter, M. J.; Lupton, J. M. Formation of a Defect-Free π-Electron System in Single β-Phase Polyfluorene Chains. *J. Am. Chem. Soc.* **2011**, *133*, 3690–3692.
37. Chang, R.; Hsu, J. H.; Fann, W. S.; Liang, K. K.; Chang, C. H.; Hayashi, M.; Yu, J.; Lin, S. H.; Chang, E. C.; Chuang, K. R.; *et al.* Experimental and Theoretical Investigations of Absorption and Emission Spectra of the Light-Emitting Polymer MEH−PPV in Solution. *Chem. Phys. Lett.* **2000**, *317*, 142–152.
38. Jiu, T. G.; Li, Y. L.; Liu, X. F.; Liu, H. B.; Li, C. H.; Ye, J. P.; Zhu, D. B. Molecular Modeling of Poly(*p*-phenylenevinylene): Synthesis and Photophysical Properties of Oligomers. *J. Polym. Sci. A1* **2007**, *45*, 911–924.
39. Peteanu, L. A.; Sherwood, G. A.; Werner, J. H.; Shreve, A. P.; Smith, T. M. Visualizing Core−Shell Structure in Substituted PPV Oligomer Aggregates Using Fluorescence Lifetime Imaging Microscopy (FLIM). *J. Phys. Chem. C* **2011**, *115*, 15607–15616.
40. Walker, A. B.; Kambili, A.; Martin, S. J. Electrical Transport Modelling in Organic Electroluminescent Devices. *J. Phys.-Condens. Mater.* **2002**, *14*, 9825–9876.